Marine and Petroleum Geology 86 (2017) 52–65

Contents lists available at ScienceDirect

Marine and Petroleum Geology

journal homepage: www.elsevier.com/locate/marpetgeo

Research paper

Petrographic and geochemical characteristics of the lacustrine black shales from the Upper Triassic Yanchang Formation of the Ordos Basin, China: Implications for the organic matter accumulation

Cheng Wang [a, d], Qinxian Wang [a, *], Guojun Chen [b], Long He [a, d], Yong Xu [b, d], Linying Chen [c], Duofu Chen [a, c, **]

[a] CAS Key Laboratory of Ocean and Marginal Sea Geology, Guangzhou Institute of Geochemistry, Chinese Academy of Sciences, Guangzhou 510640, China
[b] Key Laboratory of Petroleum Resources Research, Chinese Academy of Sciences, Lanzhou 730000, China
[c] Shanghai Engineering Research Center of Hadal Science and Technology, College of Marine Sciences, Shanghai Ocean University, Shanghai 201306, China
[d] University of Chinese Academy of Sciences, Beijing 100049, China

ARTICLE INFO

Article history:
Received 8 October 2016
Received in revised form
25 March 2017
Accepted 9 May 2017
Available online 11 May 2017

Keywords:
Black shale
Organic matter accumulation
Primary productivity
Redox conditions
Sedimentation rate
Volcanic ash
Upper Triassic
Ordos basin

ABSTRACT

The lacustrine black shales in the Chang7 Member from the Upper Triassic Yanchang Formation of the Ordos Basin in Central China are considered one of the most important hydrocarbon source rocks. However, the mechanism of organic accumulation in the black shales remains controversial. To resolve the controversy, with the former paleontological data of Yanchang Formation and sedimentation rate data of the Chang7 black shales, we investigated the typical intervals of the Chang7 black shales (TICBS) which were obtained by drilling in Yaowan at the southern margin of the Ordos Basin and performed various sedimentary, isotopic and geochemical analysis, including the sedimentary petrography, pyrite morphology, total organic carbon (TOC) and total sulfur (TS), the ratio of pyritic Fe to total Fe (DOP_T), major and trace elements, together with pyritic sulfur isotopes ($\delta^{34}S_{py}$). The high sulfur content, enrichment of redox-sensitive trace metals, and the lower sedimentation rate of the TICBS in addition to the presence of marine spined acritarchs and coelacanth fossils indicate that the TICBS were deposited in a lacustrine environment possibly influenced by seawater. The petrographic observations show a thick layer of black shale with interlayers of thin layered siltstone (silty mudstone) and laminated tuff, which were related to the turbidity currents and volcanism, respectively. The U/Th, C-S, and Mo-U covariations, pyrite morphology, DOP_T, combined with the $\delta^{34}S_{py}$, suggest that the deposition occurred beneath the anoxic-sulfidic bottom waters, which was intermittently influenced by the oxygen-containing turbidity. The Ni/Al and Cu/Al possibly show extremely high to high primary productivity in the water column, which might be connected with the substantial nutrients input from seawater or frequently erupted volcanic ash entering the lake. In addition, the coincidence of an increased abundance of TOC with increased P/Al, Ni/Al, Cu/Al and U/Th, as well as relatively consistent Ti/Al suggest that the accumulation of the organic matter might be irrelevant to the clastic influx, and was mainly controlled by the high primary productivity and anoxic-sulfidic conditions. Further, the covariations of TOC vs. P/Al and TOC vs. Ba/Al indicate that the high primary productivity led to the elevated accumulation and burial of organic matter, while the anoxic to sulfidic conditions were likely resulted from an intense degradation of the organic matter during the early diagenesis. In summary, the organic matter accumulation is ultimately attributed to the high primary productivity possibly resulted from seawater or volcanic ash entering the lake.

* Corresponding author. CAS Key Laboratory of Ocean and Marginal Sea Geology, Guangzhou Institute of Geochemistry, Chinese Academy of Sciences, Guangzhou 510640, China.
** Corresponding author. Shanghai Engineering Research Center of Hadal Science and Technology, College of Marine Sciences, Shanghai Ocean University, Shanghai 201306, China.
E-mail addresses: qinxianwang@gig.ac.cn (Q. Wang), cdf@gig.ac.cn (D. Chen).

http://dx.doi.org/10.1016/j.marpetgeo.2017.05.016
0264-8172/

1. Introduction

The deposition of black shales and the accumulation of organic matter in black shales not only involves the basic biogeochemical processes on Earth, including photosynthesis, oxidation, bacterial sulfate reduction and humification, etc., but also makes an important contribution to the primary source of hydrocarbons and other economic mineral deposits (Arthur and Sageman, 1994; Hedges and Keil, 1995; Burdige, 2007). The preservation and enrichment of the organic matter in the sediments is controlled by many factors, such as primary productivity, bottom-water oxygen supply, nutrient availability, clastic influx and the activity of such degradation processes as bacterial sulfate reduction (e.g. Demaison and Moore, 1980; Pedersen and Calvert, 1990; Murphy et al., 2000; Wei et al., 2012; Lash and Blood, 2014; Fu et al., 2015; Yan et al., 2015). However, the most important factors are attributed to primary productivity, redox conditions, and sedimentation rate. Correspondingly, three “simple” models on the accumulation of organic matter have been proposed, including the models on productivity, preservation and sedimentation rate (Katz, 2005). The productivity model suggests that a high level of primary productivity, which is induced by a high nutrient supply from the sedimentary environments, results in a large accumulation of organic matter (Pedersen and Calvert, 1990; Hay, 1995; Parrish, 1995). The preservation model argues that bottom dysoxia/anoxia ought to be regarded as the main control on organic matter preservation, which enhances organic matter accumulation by limiting the benthic activity and reducing the consumption of organic matter (Demaison and Moore, 1980). The sedimentation rate model suggests that there is a critical threshold in the sedimentation rate (Ibach, 1982). When the sedimentation rate is below this threshold, the oxidation and bioturbation of the organic matter potentially decrease with increasing sedimentation rate. However, above this threshold, as the sedimentation rate continues to increase, the dilution of organic matter increases whilst the amount of accumulated organic matter decreases. Therefore, it is difficult to explain organic accumulation with a single factor in all sediments and different sedimentary settings may have specific factors that control the accumulation of organic matter (Arthur and Sageman, 1994; Canfield, 1994; Rimmer et al., 2004; Yan et al., 2015; Zeng et al., 2015).

The lacustrine black shales in the Chang7 Member from the Upper Triassic Yanchang Formation of the Ordos Basin, Central China, have a high abundance of organic matter with a strong potential for hydrocarbon generation and expulsion (Yang and Zhang, 2005). The preservation of a large amount of cyanobacteria, green algae and acritarchs shows that the productivity was high during the deposition of the shales (Ji et al., 2012). Laminated black shales, biomarkers and trace elements indicate that the Chang7 black shales were deposited in an anoxic setting (Yang and Zhang, 2005; Zhang et al., 2008; Yang et al., 2010; Qiu et al., 2014). Further, volcanic eruptions and lake-bottom hydrothermal activities during the same periods may have been the sources for significant nutrients, resulting in an enhanced biological productivity (Qiu et al., 2009b; Zhang et al., 2009, 2010). Lastly, the identification of marine spined acritarchs and coelacanth fossils from the Chang7 black shales suggest conditions with a marine influence (Su, 1984; Xu et al., 2003). Despite previous studies dealing with the Chang7 black shales, the factors controlling the enrichment of organic matter are not well understood. Further, the hypothesis of marine incursion events is not generally accepted and it is even unclear whether those events have influenced the accumulation of organic matter in shales.

Using traditional sedimentology and sediment geochemistry in conjunction with the published data of paleontology and sedimentation rate, we re-evaluate the depositional environment of the Yanchang Formation and re-assess various sediment parameters pertaining to the typical intervals of the Chang7 black shales (TICBS). By so doing, we explored the mechanism of organic matter accumulation and factors controlling the deposition of the TICBS.

2. Geological background, samples and analytical methods

The Ordos Basin spans five provinces namely, Shaanxi, Gansu, Ningxia, Inner Mongolia and Shanxi, and is a multicycle cratonic basin (Yang and Zhang, 2005). It has a significant resource potential, amounting to about one-third of China's total oil and gas production (Yang et al., 2013). The Ordos Basin has experienced different stages of evolution, including the Early Paleozoic marginal ocean basin, Early to the Late Paleozoic littoral basin, Late Permian to Middle Triassic large interior basin and Late Triassic to the Early Cretaceous para-foreland basin, before finally developing into the tectonic framework of the current basin. In the foreland basin stage during the Late Triassic, the North China plate and Yangtze plate collided and integrated, resulting in the closure of the relict of Youjiang and Qinling troughs and the formation of the Qinling Mountains (Yang, 2002). The tectonic process provided a large depositional space for the Ordos Basin (Liu, 1998; Liu and Yang, 2000) and subsequently deposited a set of fluvial-lacustrine sediments with a thickness of about 1300 m - the Upper Triassic Yanchang Formation (Deng et al., 2008). It is subdivided into 10 members from bottom to top (Qiu et al., 2010) and the depositional period of Chang7 was the pinnacle of the basin development. Meanwhile, intense subsidence allowed large-scale deposition of organic-rich source rocks in the deep to semi-deep water of the lake (Yang and Zhang, 2005). The Chang7 member can be subdivided into 3 sub-members based on the sedimentary cycles, named Chang7_1 to Chang7_3 from top to bottom. Chang7_3 is mainly a developed, thick layer of oil shale with tuff layers at the bottom, Chang7_2 has developed mudstone with thin tuff intercalations in the lower part and development of silty mudstone in the upper part, and lastly Chang7_1 is mainly composed of mudstone and silty mudstone (Qiu, 2011).

The well Yaowan 1 (N35° 13'; E109° 01′) lies in the Tongchuan area at the southern margin of the Ordos Basin, which is 35 km north of Tongchuan City (Fig. 1A). The total thickness of the drilled core is 168 m including the Chang6, Chang7 and Chang8 strata of the Yanchang Formation. The Chang6 and Chang8 strata are mainly thick-bedded fine-grained gray-green sandstone, whereas the Chang7 strata are predominantly black shale and siltstone with intercalations of gray mudstone, silty mudstone, and tuff. In this paper, we collected samples from the typical intervals of black shales (108.5–117.5 m with the total length of 9 m) mostly developed in Chang7_2. The sampling interval is from 0.3 to 0.5 m with a total of 25 samples (Fig. 1B; Table 1).

Thin sections of sedimentary rock samples were prepared at the Guangzhou Institute of Geochemistry, Chinese Academy of Sciences, and were studied in detail using an optical microscope (Leica DMRX 888056) and a scanning electron microscope (SEM; Carl Zeiss SUPRA55 SAPPHIRE). Powdered samples were taken from the drilled core using a hand-held dental drill (ROTEX™ 782E), and care was taken to avoid mixing those powders with tuff and phosphate nodules, and subsequently, samples were pulverized to <200 mesh sizes with an agate mortar.

Major and trace elements were measured at the Institute of Geochemistry, Chinese Academy of Sciences. Powdered samples were placed in Teflon beakers and dissolved in 1 mL of hydrofluoric acid (HF) and 1 mL of nitric acid (HNO_3). Subsequently, the sealed beakers were placed into an electric oven and heated to 185 °C for

about 36 h. Thereafter, the solutions were evaporated on a hot plate overnight and then treated with 2 mL of HNO_3 and 3 mL of ultrapure distilled water. The beakers were sealed again and heated to 135 °C for about 5 h to dissolve the residue. Major and trace elements were determined using a Varian Vista Pro ICP-AES and a Perkin-Elmer Sciex ELAN 6000 ICP-MS following the method described by Qi et al. (2005). Certified reference materials (GSR-1, OU-6, 1633-a, GXR-2, GXR-5) were used for quality control. The precision and accuracy were both above 5% for Al, Ti, P, Fe, Ba, Cu, Ni, Th, U, and 10% for Mo.

The total organic carbon (TOC) and total sulfur (TS) contents were measured using a vario EL cube elemental analyzer at the Guangzhou Institute of Geochemistry, Chinese Academy of Sciences. At first, the total carbon and total sulfur contents were measured. Secondly, samples were decalcified with 6 mol/L HCl to remove inorganic carbon, and were washed twice with de-ionized water before dried at 60 °C for TOC determination. Certified reference material (sulfanilamide) was used for quality control. The precision and accuracy of the TOC and TS measurements were both above 0.5%.

Sulfur isotopic measurement was conducted by the Oxy-Anion Stable Isotope Consortium (OASIC) at Louisiana State University. Firstly, the sample split was treated with 1 M chromium dichloride ($CrCl_2$) solution and 6 N hydrochloric acid (HCl) + 10 mL alcohol. The hydrogen sulfide was immediately purged by nitrogen stream and was trapped and collected in a zinc acetate (ZnAc) solution to which 2% silver nitrate ($AgNO_3$) +6 N ammonium hydroxide (NH_4OH) solutions were added to precipitate silver sulfide (Ag_2S), which was then filtered, rinsed and dried. All these procedures were based on the method of Canfield et al. (1986). Afterward, the dried Ag_2S was mixed with vanadium pentoxide (V_2O_5) and then converted to sulfur dioxide (SO_2) by combustion with an elemental analyzer at 980 °C. Finally, the sulfur isotopic ratio of the purified SO_2, namely, the pyrite sulfur isotope value ($\delta^{34}S_{py}$), was analyzed by using a Finnigan Delta-S mass spectrometer. The standard deviation associated with the $\delta^{34}S$ analysis was ±0.3‰ and was reported according to the VCDT (Vienna Canyon Diablo Troilite) standard.

3. Results

3.1. Petrographic characteristics

The TICBS from well Yaowan 1 is thick, with interlayers of thin siltstone (silty mudstone) and laminated tuff. The interlayers of siltstone and silty mudstone are rare compared to the tuff interlayers and they often abruptly shift to black shale at the bottom with a flame-like sedimentary structure (Fig. 2A), which is considered to be the characteristic of deepwater deposits formed by turbidity currents (Feng et al., 2012; Qiu, 2011). The interlayers of tuff developed in the whole shales are mainly ash lamina, which is usually a centimeter to less than a millimeter. Phosphate nodules are often found above ash lamina (Fig. 2B and D).

Under the single-polar microscope, the ash lamina are composed of coarse crystal fragments of plagioclase which are scattered in the matrix of tiny volcanic dust. The contents of the crystal fragments of plagioclase are 50–70% with a particle size of about 0.05–0.3 mm (Fig. 2C). In addition, there are usually small amounts of volcanic crystal fragments found in the organic lamina (Fig. 2C).

3.2. The characteristics of TOC, TS, and $\delta^{34}S_{py}$

The TOC and TS contents of the black shales are both high and highly variable, ranging from 7.21% to 32.28% (avg. 18.35%), and 3.84%–16.83% (avg. 7.57%), respectively. The TOC and TS contents of siltstones and silty mudstones are relatively low with small variations, ranging from 2.84% to 4.27% (avg. 3.55%) and 0.58%–1.94% (avg. 1.16%), respectively (Fig. 3; Table 1).

The $\delta^{34}S_{py}$ of the TICBS range between −2.4‰ and +8.7‰, with the majority being positive. The $\delta^{34}S_{py}$ fluctuate significantly in the profile and are generally lower in the black shales with high TOC contents (Fig. 3).

3.3. The characteristics of major and trace elements

The aluminum (Al) and titanium (Ti) contents of the TICBS are relatively variable with the similar trends (Fig. 3). The Ti/Al is relatively steady, while the Ti/Al of siltstones and silty mudstones (0.036–0.061, avg. 0.049) are slightly higher than those of the associated black shales (0.025–0.058, avg. 0.043) (Fig. 3; Table 1).

To eliminate the influence of terrigenous clastics, the productivity indicators, including phosphorus (P), barium (Ba), nickel (Ni) and copper (Cu) are normalized to aluminum (Al) (Algeo and Tribovillard, 2009). The profiles of the P/Al, Ni/Al and Cu/Al of the TICBS correlate well, with the Ba/Al showing a different trend (Fig. 4). Generally, the mean P/Al, Ni/Al and Cu/Al of the black shales (131.5×10^{-4}, 7.89×10^{-4} and 22.89×10^{-4}) are significantly higher than those of the siltstones and silty mudstones (85.79×10^{-4}, 2.74×10^{-4} and 5.92×10^{-4}; one anomaly is the sample A-24 with extremely high P/Al, mostly likely caused by phosphate nodules in the shales). Meanwhile, the mean Ba/Al is lower than those of the black shales (73.86×10^{-4}) compared to the siltstones and silty mudstones (97.70×10^{-4}) (Table 1).

The enrichment factor (M_{EF}) is used to describe the degree of element enrichment in shale, which is calculated according to the following equation: $M_{EF}=(X/Al)_{sample}/(X/Al)_{PAAS}$, where X and Al represent the concentration of elements X and Al, respectively. Samples are normalized using the post-Archean average shale (PAAS) of McLennan (1989). $M_{EF}>1$ represents an element enrichment to the PAAS concentrations, $M_{EF}>3$ represents a detectable enrichment and $M_{EF}>10$ indicates a moderate to a strong degree of enrichment (Algeo and Tribovillard, 2009). The enrichment factors of phosphorus (P), iron (Fe), molybdenum (Mo), uranium (U), barium (Ba), thorium (Th), nickel (Ni) and copper (Cu) (P_{EF}, Fe_{EF}, Mo_{EF}, U_{EF}, Ba_{EF}, Th_{EF}, Ni_{EF} and Cu_{EF}) of the TICBS are shown in Table 1 and Fig. 5. In the black shales, the Mo and U are strongly enriched, Fe and Cu are detectably enriched, while the other elements show minor to no enrichment. In siltstones and silty mudstones, the Mo has a detectable to moderate enrichment, P, U, Ba, and Cu show slight enrichment, Fe, and Th show no enrichment, and Ni is depleted.

4. Discussion

4.1. The depositional setting: lacustrine or marine?

It is generally believed that the major basins in central and western China, including the Ordos Basin, have been transformed from sea-land interaction (marine or offshore lake) into a freshwater lake in Late Permian (Ji et al., 2006). However, marine fossils were found in the Late Triassic sediments from the southwestern Ordos Basin. For example, a typical marine coelacanth fossil with a rounded tail was found in the Chang3^3 (Chang4-6) of the Upper Triassic Yanchang Formation in Huachi area (Liu et al., 1999); a broken marine coelacanth fossil was discovered in the Tongchuan Formation (Chang7) in Tongchuan area (Su, 1984); spined acritarchs fossils belonging to marine planktonic algae were identified in the Chang2, 3, 6 and 7 members of the Upper Triassic Yanchang Formation in the southwestern of the Ordos basin (Xu et al., 2003;

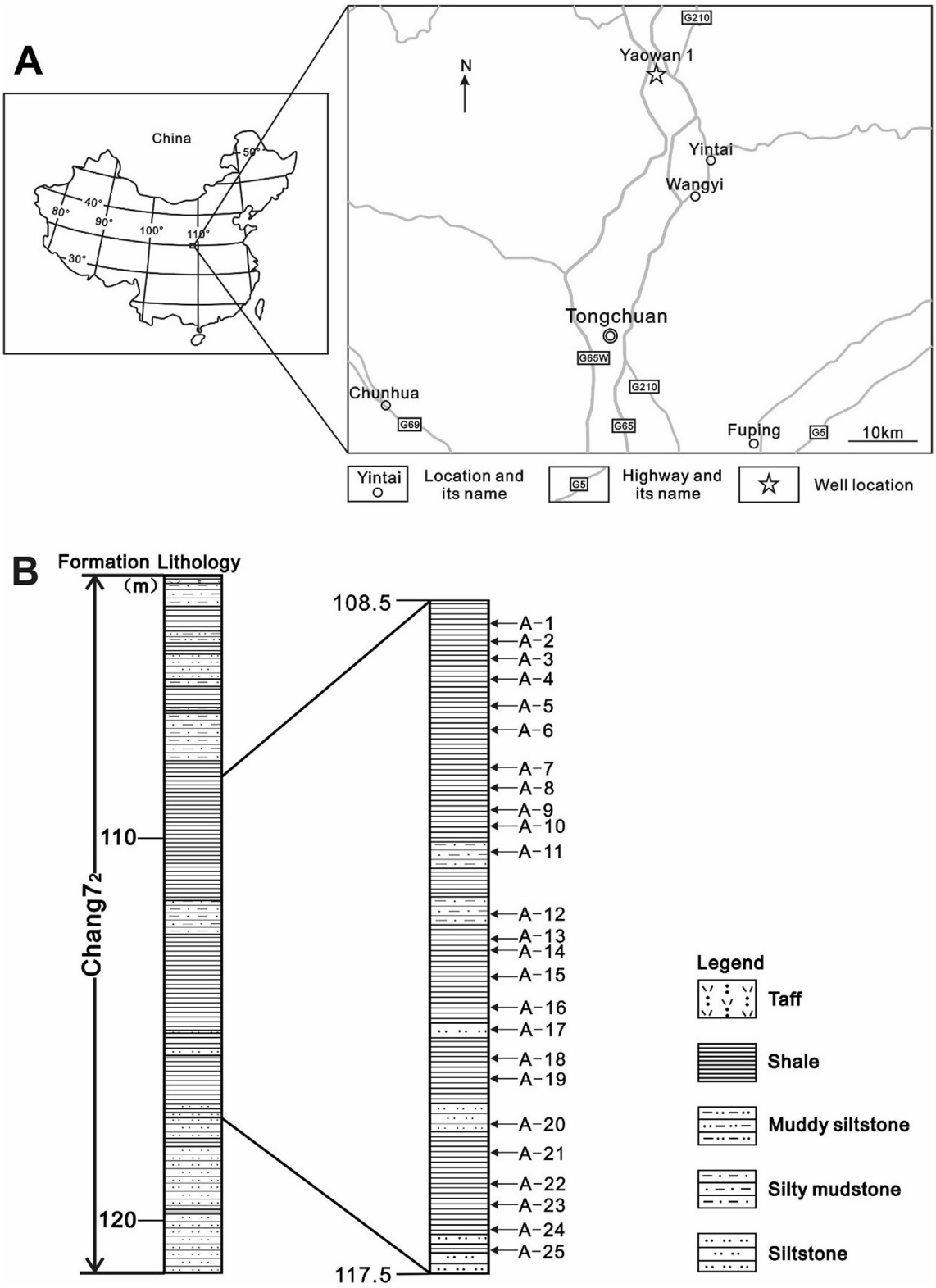

Fig. 1. (A) Study site (left) and an expanded view (right) of the Tongchuan area with the location of well Yaowan 1; and (B) Vertical profile in which lithologies of the Chang7_2 strata and the position of samples in this study are shown.

Ji et al., 2006). In addition, the high sulfur content (avg.6.54%, Max >15, Fig. 3), the enrichment of Mo, U and other redox-sensitive trace metals (Fig. 5) of the TICBS suggest the characteristics of the marine environment (Berner and Raiswell, 1984; Rimmer, 2004). Lastly, the sedimentation rate of Chang7 shales is in the range of limited marine basins (see below section 4.4 for discussion). Therefore, it is possible that seawater intruded into the Ordos Basin, and some sediments of the Yanchang Formation

Table 1
Variation of the multiple geochemical parameters of the samples from the typical intervals of the Chang7 black shales.

Samples	Depth(m)	Lithology	TOC (%)	TS (%)	Al (%)	Ti (%)	Fe (%)	P (ug/g)	Mo (ug/g)	U (ug/g)	Ba (ug/g)	Th (ug/g)	Ni (ug/g)	Cu (ug/g)
A-1	108.80	Black shale	31.66	7.71	4.81	0.19	7.40	982.8	80.7	50.5	344.0	10.4	40.7	131.0
A-2	109.00	Black shale	10.59	3.84	8.09	0.20	4.37	513.4	34.7	32.1	408.0	15.7	26.8	67.6
A-3	109.25	Black shale	17.59	6.26	6.37	0.27	6.65	730.5	55.6	53.0	391.0	11.6	44.9	113.0
A-4	109.50	Black shale	24.80	7.51	5.75	0.26	7.31	1260.0	90.5	73.6	431.0	10.4	53.6	127.0
A-5	109.85	Black shale	7.21	4.44	8.69	0.50	4.18	615.5	23.9	27.9	931.0	14.8	25.2	73.8
A-6	110.20	Black shale	15.21	5.36	5.65	0.30	5.94	567.0	26.9	20.2	377.0	13.2	51.2	79.4
A-7	110.70	Black shale	14.02	9.36	4.74	0.23	8.55	328.1	64.0	59.4	383.0	9.1	33.6	145.0
A-8	110.95	Black shale	26.79	11.27	4.05	0.17	9.92	708.5	94.1	52.0	248.0	7.4	47.2	183.0
A-9	111.25	Black shale	32.28	8.27	3.75	0.17	6.98	1093.0	57.7	44.9	280.0	7.2	30.4	101.0
A-10	111.45	Black shale	14.55	8.58	6.01	0.24	8.32	561.7	40.5	49.8	325.0	12.5	41.3	109.0
A-11	111.80	Silty mudstone	3.83	0.95	8.11	0.29	5.11	701.4	7.1	10.0	583.0	13.2	23.1	47.5
A-12	112.65	Silty mudstone	4.27	1.15	7.24	0.44	2.98	906.5	12.8	9.8	697.0	14.2	30.1	70.0
A-13	113.00	Black shale	10.96	5.97	6.99	0.27	6.82	490.4	37.2	30.0	350.0	12.5	81.0	108.0
A-14	113.10	Black shale	9.08	3.97	7.35	0.29	6.65	440.5	27.4	22.2	366.0	13.9	39.4	74.8
A-15	113.45	Black shale	9.81	7.21	7.41	0.31	7.28	425.4	48.6	53.7	449.0	12.4	42.6	97.8
A-16	113.90	Black shale	19.86	8.11	3.27	0.16	7.22	516.2	55.9	34.5	228.0	7.6	31.2	104.0
A-17	114.20	Siltstone	2.84	1.94	9.18	0.53	2.68	519.1	6.0	4.2	1210.0	12.4	7.2	19.6
A-18	114.60	Black shale	17.71	10.52	4.63	0.21	9.48	375.0	96.7	33.6	300.0	7.0	32.5	132.0
A-19	114.85	Black shale	17.08	4.78	5.36	0.27	5.12	527.9	36.0	32.4	396.0	10.1	53.3	85.1
A-20	115.40	Siltstone	3.27	0.58	7.50	0.30	2.50	560.6	4.4	4.4	680.0	10.1	23.8	45.2
A-21	115.80	Black shale	29.90	16.83	2.66	0.12	14.36	509.2	99.4	66.4	223.0	5.6	39.6	165.0
A-22	116.20	Black shale	17.51	8.98	4.68	0.21	7.79	856.4	61.5	54.5	396.0	6.7	28.0	107.0
A-23	116.50	Black shale	19.00	7.94	5.60	0.22	7.39	960.3	55.7	57.0	389.0	10.6	41.8	112.0
A-24	116.80	Black shale	19.08	7.29	5.53	0.21	6.91	5484.0	59.5	80.8	609.0	8.8	33.3	124.0
A-25	117.15	Black shale	20.67	4.77	5.71	0.20	4.97	898.6	60.5	37.6	750.0	7.7	47.5	112.0

Ti/Al	P/Al ($\times 10^{-4}$)	Ba/Al ($\times 10^{-4}$)	Ni/Al ($\times 10^{-4}$)	Cu/Al ($\times 10^{-4}$)	P_{EF}	Fe_{EF}	Mo_{EF}	U_{EF}	Ba_{EF}	Th_{EF}	Ni_{EF}	Cu_{EF}	U/Th	$\delta^{34}S_{py}$ (‰)	DOPT
0.040	204.49	71.58	8.47	27.26	2.92	3.06	168.09	33.90	1.10	1.48	1.54	5.46	4.85	3.2	0.91
0.025	63.46	50.43	3.31	8.36	0.91	1.07	42.93	12.82	0.78	1.33	0.60	1.67	2.05	0.4	0.77
0.042	114.75	61.42	7.05	17.75	1.64	2.08	87.43	26.88	0.95	1.25	1.28	3.55	4.57		0.82
0.045	219.10	74.95	9.32	22.08	3.13	2.53	157.53	41.31	1.15	1.24	1.70	4.42	7.07	−2.4	0.90
0.057	70.82	107.12	2.90	8.49	1.01	0.96	27.53	10.36	1.65	1.17	0.53	1.70	1.88	7.9	0.93
0.053	100.30	66.69	9.06	14.05	1.43	2.09	47.63	11.56	1.03	1.60	1.65	2.81	1.53	4.1	0.79
0.048	69.21	80.78	7.09	30.58	0.99	3.59	135.11	40.43	1.24	1.31	1.29	6.12	6.54		0.96
0.042	174.99	61.25	11.66	45.20	2.50	4.88	232.65	41.51	0.94	1.24	2.12	9.05	7.08	0.3	0.99
0.046	291.30	74.62	8.10	26.92	4.17	3.70	153.93	38.68	1.15	1.32	1.47	5.39	6.24		1.04
0.041	93.43	54.06	6.87	18.13	1.34	2.75	67.44	26.76	0.83	1.43	1.25	3.63	3.99		0.90
0.035	86.52	71.92	2.85	5.86	1.24	1.26	8.82	3.99	1.11	1.12	0.52	1.17	0.76		0.16
0.061	125.28	96.33	4.16	9.67	1.79	0.82	17.71	4.38	1.48	1.35	0.76	1.94	0.69	3.4	0.34
0.038	70.20	50.10	11.60	15.46	1.00	1.94	53.31	13.87	0.77	1.23	2.11	3.10	2.40		0.77
0.040	59.93	49.79	5.36	10.18	0.86	1.80	37.31	9.73	0.77	1.30	0.98	2.04	1.59	−1.3	0.52
0.042	57.44	60.63	5.75	13.21	0.82	1.96	65.69	23.43	0.93	1.15	1.05	2.64	4.33		0.87
0.050	157.96	69.76	9.55	31.82	2.26	4.40	171.21	34.04	1.07	1.59	1.74	6.37	4.54	1.3	0.98
0.057	56.57	131.85	0.78	2.14	0.81	0.58	6.58	1.47	2.03	0.93	0.14	0.43	0.34	8.7	0.63
0.044	81.08	64.86	7.03	28.54	1.16	4.08	209.28	23.46	1.00	1.04	1.28	5.71	4.79	3	0.97
0.050	98.46	73.87	9.94	15.87	1.41	1.90	67.22	19.54	1.14	1.29	1.81	3.18	3.21		0.82
0.040	74.78	90.71	3.17	6.03	1.07	0.66	5.89	1.91	1.40	0.92	0.58	1.21	0.44	1.7	0.20
0.044	191.35	83.80	14.88	62.01	2.74	10.74	373.92	80.52	1.29	1.44	2.71	12.41	11.87	0.7	1.03
0.044	182.93	84.58	5.98	22.85	2.62	3.31	131.49	37.58	1.30	0.98	1.09	4.58	8.16	3.4	1.01
0.039	171.46	69.45	7.46	20.00	2.45	2.63	99.55	32.88	1.07	1.30	1.36	4.00	5.38		0.94
0.038	991.43	110.10	6.02	22.42	14.18	2.49	107.67	47.15	1.70	1.09	1.10	4.49	9.17	3.7	0.92
0.036	157.32	131.30	8.32	19.61	2.25	1.73	106.02	21.27	2.02	0.93	1.51	3.93	4.88		0.84

(including Chang7) might have marine deposits with the characteristics of offshore lakes in the Late Triassic.

However, it has been debated regarding the origin of seawater. Liu et al. (1999) proposed that (1) the trough of northern margin of the Ordos Basin has been closed in the late Permian; (2) there was no seawater connected from the eastern and southern margin of the Ordos Basin after the Permian as indicated by the regular sedimentary sequence of regression from eastern and southern margin into interior of the Ordos Basin; (3) the northern part of the western basin margin is a set of coarse debris continental sediments in the Permian and Triassic while the southern part of the western basin margin has Early to Middle Triassic marine strata (Fig. 6). Taking into consideration of all the evidence it is suggested that the Ordos Basin was possibly connected to the sea in the southwest margin.

4.2. Redox conditions

4.2.1. Pyrite morphology and DOP_T

Pyrite framboid diameter is a potential tool to distinguish anoxic-euxinic conditions from oxic-dysoxic conditions (Wilkin and Barnes, 1997; Wignall and Newton, 1998; Riquier et al., 2006). Wilkin and Barnes (1996) suggested the mean framboid diameter (±1σ, σ stands for standard deviation) from sediments of anoxic-euxinic and oxic-dysoxic environments are 5.0 ± 1.7 μm and 7.7 ± 4.1 μm, respectively. They also think fewer than 4% of framboids are >10 μm in euxinic sediments; generally 10–50% of framboids are >10 μm in non-euxinic sediments. The size distributions of framboidal pyrite from the black shales of the TICBS is 4–8 μm with rather constant and small sizes, and only a few of those framboidal pyrite (<10%) are >10 μm (Fig. 7 A, B and D).

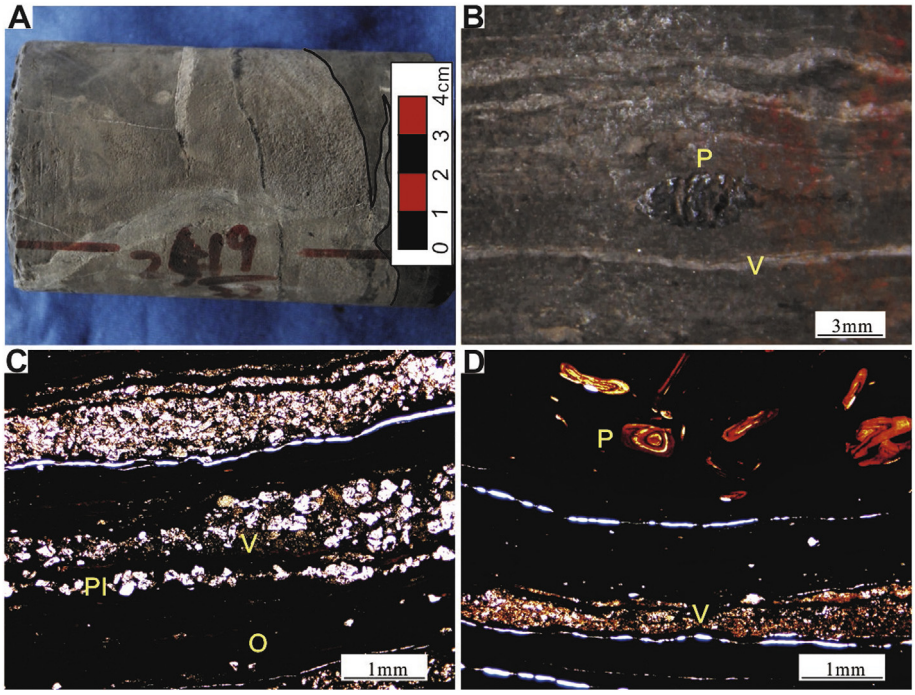

Fig. 2. Characteristics of the TICBS. (A) Black shale and turbidite siltstone with a flame-like sedimentary structure (black line); (B) Volcanic ash layers (light-colored layer marked "V") and phosphate nodule (dark nodule marked "P") developed in the black shale samples; (C) Organic matter lamina (dark layer marked "O") and millimeter thin volcanic ash layer (bright layer marked "V") in which the crystals are plagioclase (sample A-24); (D) Phosphate nodules (brown nodule marked "P") and volcanic ash layer (the bright layer marked "V") of sample A-24. The fine bright bands in C and D are fractures, artefacts produced by the process of making thin sections. Note that A and B are sample photographs, and C and D are photographs taken under the single-polar microscope. (For interpretation of the references to colour in this figure legend, the reader is referred to the web version of this article.)

Therefore, the black shales were possibly deposited in anoxic-euxinic bottom water. In contrast to the shales, the siltstones and silty mudstones have a few pyrite framboids and often 30% of framboids are >10 μm (Fig. 7C), which likely indicate the oxic-dysoxic environment.

The degree of pyritization (DOP), a ratio of pyritic Fe to total reactive Fe within a sample, is used as a paleoredox proxy (Raiswell et al., 1988). Generally, DOP <0.42 indicates an oxic, 0.46 < DOP<0.75 the suboxic, and DOP>0.75 anoxic-euxinic environment (Raiswell et al., 1988; Sageman et al., 2003). The DOP_T, the ratio of pyritic Fe (based on total S) to total Fe, can be used in place of the true DOP values, if pyrite S composes the bulk of total S and reactive Fe compose the bulk of total Fe (Algeo and Maynard, 2008; Algeo et al., 2008b). This is true for many black shale formations including the Pennsylvanian shales, Appalachian Basin Devonian black shales, and Late Triassic Chang7 shales (Rimmer et al., 2004; Algeo and Maynard, 2008; Yuan et al., 2016b). In current study, the DOP_T of the shales is between 0.52 and 1.04 (Fig. 4), almost all of them higher than 0.75, which suggests an anoxic-euxinic environment. In contrast to the shales, the DOP_T of the siltstones and

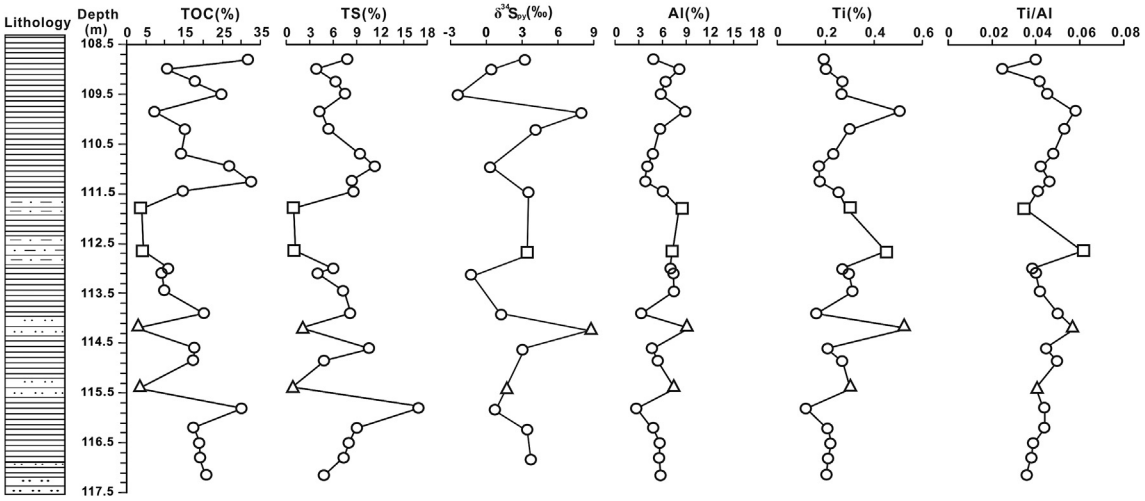

Fig. 3. Down-core variations of TOC contents, TS contents, $\delta^{34}S_{py}$ ratios, Al contents, Ti contents and Ti/Al ratios of the TICBS. Unfilled circles, squares, and triangles represent black shales, silty mudstones, and siltstones, respectively.

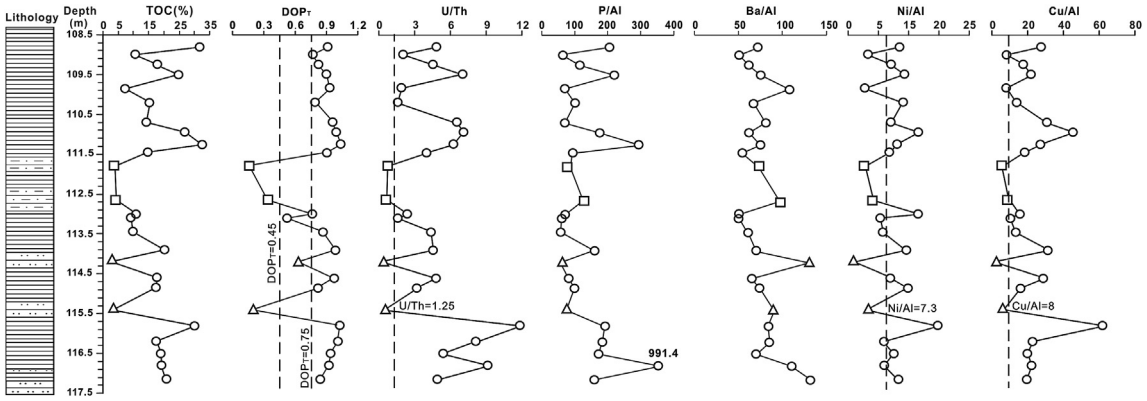

Fig. 4. Down-core variations of the TOC contents, DOP_T, U/Th, P/Al ($\times 10^{-4}$), Ba/Al ($\times 10^{-4}$), Ni/Al ($\times 10^{-4}$) and Cu/Al ($\times 10^{-4}$) of the TICBS. The five vertical dashed lines mark in DOP_T, U/Th, Ni/Al ($\times 10^{-4}$) and Cu/Al ($\times 10^{-4}$) panels at 0.45, 0.75, 1.25, 7.3, and 8.0, respectively (Raiswell et al., 1988; Wignall and Twitchett, 1996; Böning et al., 2012). Unfilled circles, squares, and triangles represent black shales, silty mudstones and siltstones, respectively.

silty mudstones range from 0.16 to 0.62 (Fig. 4), which indicates an oxic-suboxic environment.

4.2.2. U/Th

Under oxidizing conditions, Th exists as insoluble Th^{4+}, and U exists as the dissolved form of U^{6+}. Under strong reducing conditions, Th is still in the insoluble form Th^{4+}, but U transforms from the dissolved state of U^{6+} to insoluble U^{4+}, and is enriched in sediments (Wignall and Twitchett, 1996; Kimura and Watanabe, 2001). Therefore, the U/Th are typically greater than 1.25 in an anoxic environment and less than 0.75 in an oxygen-enriched environment (Wignall and Twitchett, 1996). The U/Th of the black shales are greater than 1.25 with the highest value of 11.87 and its average of 5.05. In addition, the U/Th of the siltstones and silty mudstones are close to or less than 0.75 (Fig. 4; Table 1). These data indicate that the black shales were deposited in an intensely anoxic environment, while the siltstones and silty mudstones were deposited in an oxic to the suboxic environment.

4.2.3. C-S-Fe relationship

The theoretical composition of pyrite (FeS_2) is Fe 46.55 wt%, S 53.45 wt% and S/Fe = 1.15. In the Fe-S scatter plot, there is a good correlation between Fe and S (Fig. 8A solid line, $R^2 = 0.92$) and the TICBS are near the theoretical line of pyrite (Fig. 8A dotted line), indicating that the sulfur contained in the samples may almost entirely exist as pyrite (Dean and Arthur, 1989). Thus, the pyrite sulfur can be estimated by the total sulfur (Algeo and Maynard, 2004; Rimmer, 2004; Rimmer et al., 2004).

The C-S relationship in the sediments can be used to assess the oxygen level of bottom waters (Hofmann et al., 2000). It is based on the principle that organic matter is catabolized by bacteria, while sulfates are concurrently reduced by means of the bacteria sulfate reduction (BSR) to form hydrogen sulfides that react with iron so as to form pyrites in the sediment, resulting in the C-S covariation (Leventhal, 1987). In the C-S plot, sediments (rocks) deposited under the oxic conditions generally distribute along a line through the origin with S/C = 0.36 (Berner and Raiswell, 1984). In contrast to the oxic conditions, the euxinic environments with abundant reactive iron are characterized by S/C higher than 0.36 with positive intercepts on the S axis (Leventhal, 1983; Berner, 1984). The positive intercept indicates that the pyrite is formed in sulfidic water columns (Raiswell and Berner, 1985; Lyons and Berner, 1992). Additionally, the euxinic environments with limited reactive iron are characterized by a fairly constant or relatively high sulfur content independent of the organic carbon content (Hofmann et al., 2000).

The TICBS show a good correlation between C and S ($R^2 = 0.57$), and their trend line with a positive intercept (Fig. 8B solid line a) is close to the line of S/C = 0.36 (Fig. 8B dotted line). This shows that the TICBS may be deposited in an environment crossing from oxic to anoxic, even to sulfidic. If the samples from the siltstone and silty mudstone were excluded, the correlation between C and S becomes worse ($R^2 = 0.34$), still with a positive intercept (Fig. 8B solid line b), and a relatively high S content, indicating the sedimentary characteristics of anoxic to sulfidic environment with limited reactive iron. In summary, the black shales may have been deposited in an anoxic to the sulfidic environment, while the siltstones and silty mudstones may have been deposited in an oxic to the suboxic environment.

4.2.4. Mo-U covariation

U and Mo are redox indicators with minimal detrital influences and can truly reflect the redox conditions during sediment deposition (Tribovillard et al., 2006). As the U enrichment begins under suboxic conditions (Fe^{3+} is transforming to Fe^{2+}), whereas Mo enrichment requires the presence of H_2S (i.e., euxinic conditions) and the redox cycle of Mo potentially being influenced by particulate shuttles, the patterns of U-Mo covariations have been shown to be particularly useful proxies for paleoenvironmental reconstruction (Algeo and Tribovillard, 2009; Tribovillard et al., 2012; Luo et al., 2017).

Mo and U show strong enrichment in the black shales, whereas Mo and U shows detectable to moderate and detectable enrichment, respectively, in the siltstones and silty mudstones (Fig. 9; Table 1). Additionally, the Mo_{EF} are much higher than the U_{EF} in the black shales and slightly higher than the U_{EF} in the siltstones and silty mudstones. These data indicate that the black shales were possibly deposited in a water column with abundant H_2S, whereas siltstones and silty mudstones were deposited in water with scarce H_2S. In the diagram of the Mo-U covariation, the black shales correspond to an anoxic to the sulfidic environment, whereas the siltstones and silty mudstones correspond to an oxic to the suboxic environment (Fig. 9). Given that the siltstones and silty mudstones belongs to the turbidites (Qiu, 2011; Feng et al., 2012.), the TICBS were generally deposited in an anoxic to the sulfidic environment, but occasionally affected by the oxygen-containing turbidity.

4.2.5. Characteristics of sulfur isotopes

Studies have shown that sulfur isotopes can record changes in the redox conditions in ocean and lake systems (e.g., Strauss, 1997; Watanabe et al., 2004; Thompson and Kah, 2012). The principle is

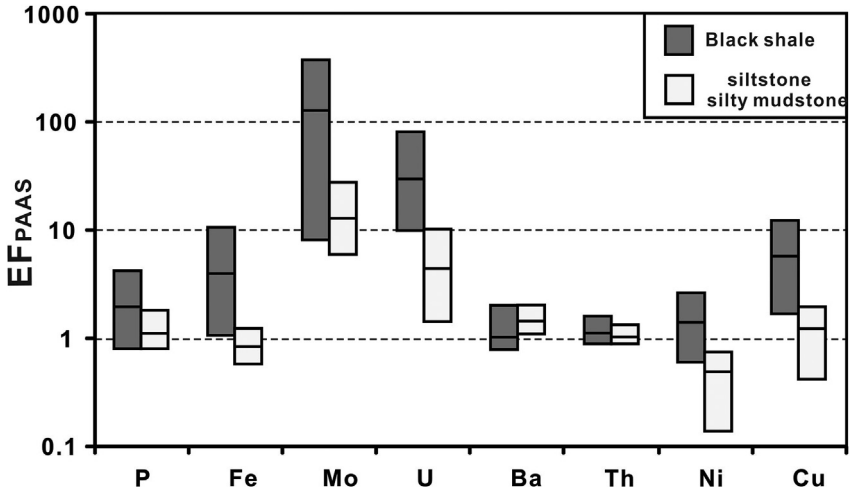

Fig. 5. Enrichment factors of some major and trace elements of the TICBS. The extent of the boxes corresponds to the range of values (min-max) and the inner line to the average values.

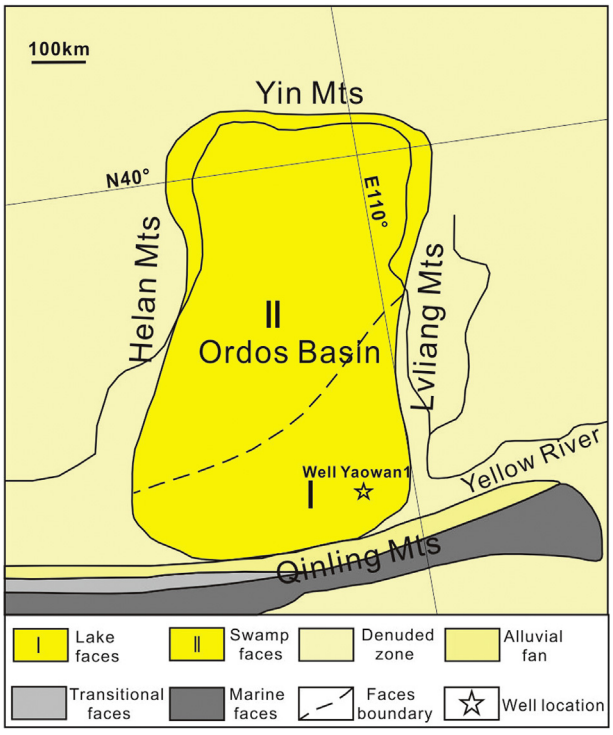

Fig. 6. Late Triassic palaeogeographic map of the Ordos Basin with well location (Modified from Qiu et al., 2009a).

that the bacterial sulfate reduction (BSR) activity induces a fractionation of the stable isotopes ^{34}S and ^{32}S, resulting in a depletion of ^{34}S in the produced sulfide relative to coeval sulfate (Kaplan and Rittenberg, 1964; Canfield, 2001). Although the sulfur isotope fractionation caused by the BSR is widespread, the degree of fractionation is ultimately controlled by the sulfate availability. In an open environment, the supply of sulfate is sufficient and the sulfur isotope fractionation is generally greater than 20–22‰ (Zaback et al., 1993; Habicht and Canfield, 1997), whereas in a closed environment, the sulfate concentration is very low and the sulfur isotope fractionation is often less than 25‰ (Schwarcz and Burnie, 1973; Chambers, 1982; Habicht and Canfield, 1996, 1997; Watanabe et al., 2004).

The $\delta^{34}S_{py}$ of the TICBS range from - 2.4 to +8.7‰ (Table 1). As the marine incursion events possibly occurred when the shales were deposited (see section 4.1), so we assume that the sulfate $\delta^{34}S$ of the Late Triassic lake water in the Ordos Basin was the same as coeval open-marine waters (15.5 ± 0.4‰; Boschetti et al., 2011), then the maximum fractionation of the sulfur isotope would be 6.4–18.3‰. It is lower than 20‰ representing the fractionation value of the sulfur isotope caused by the BSR in an open environment with sufficient sulfate, but much higher than the maximum fractionation of the sulfur isotope (4.6‰) in Late Cretaceous Songliao Basin experienced from marine incursion (Huang et al., 2013). This possibly shows that the Late Triassic Ordos Basin was a semi-closed environment, although other reasons could have caused a small S-isotope fractionations, e.g., near-quantitative consumption of water-column or porewater sulfate, more reactive (i.e., more easily metabolized) organic matter associated with greater rates of sulfate reduction (Algeo et al., 2015; Canfield, 2001).

Further, the $\delta^{34}S_{py}$ fluctuates significantly, being lighter in black shales with high TOC and heavier in black shales with low TOC or siltstones (silty mudstones) (Fig. 3). These fluctuations may possibly be related to the migration of the redox interface. It appears that when black shales with low TOC or siltstones (silty mudstones) were deposited, the redox interface was possibly located under or at the sediment-water interface, which limited the supply of sulfate in the pore water system, resulting in the formation of pyrite with heavier $\delta^{34}S_{py}$. On the other hand, when black shales with high TOC were deposited, the redox interface possibly moved up to the bottom water, which enhanced the supply of sulfate and BSR, leading to the formation of pyrite with lighter $\delta^{34}S_{py}$.

To summarize, the present data (U/Th, C-S, and Mo-U covariations, DOP_T and $\delta^{34}S_{py}$) and pyrite morphology as stated above indicate that the sediments from the TICBS, even though existing short-term oxidation to sub-oxidation, were mainly deposited in the anoxic-sulfidic depositional environment.

4.3. Primary productivity

P, Ba, Ni and Cu are potential proxies for primary productivity (Tribovillard et al., 2006). They usually represent the relative level of primary productivity and be used to compare with TOC in order to ensure the relationship between primary productivity and

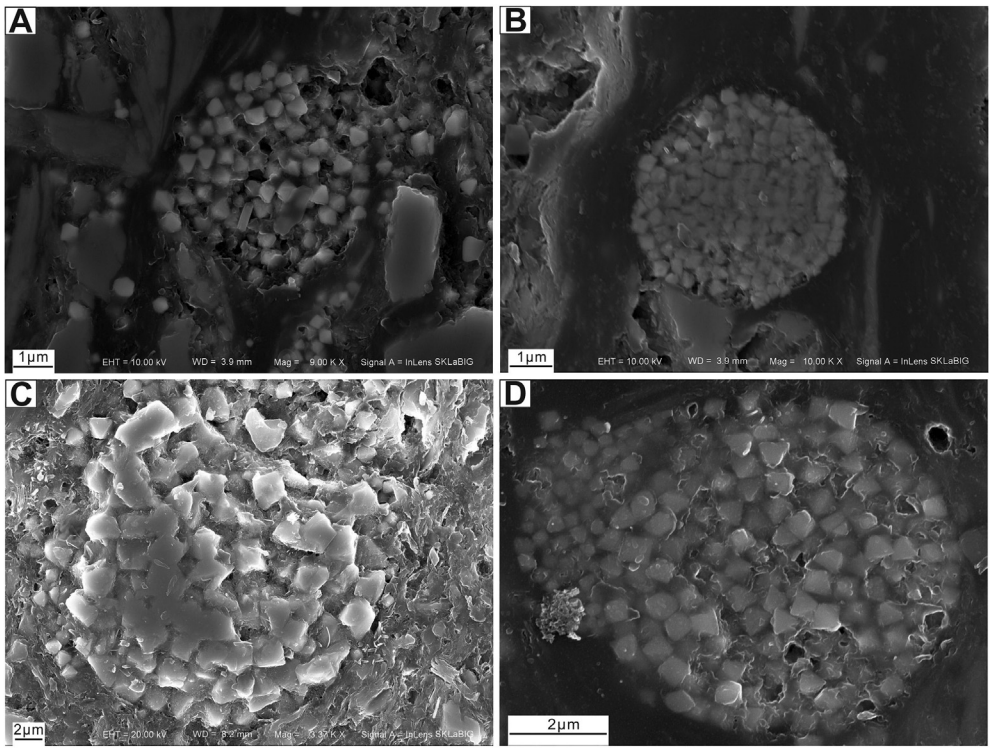

Fig. 7. Photomicrographs obtained by using a scanning electron microscope (SEM) of pyrite from studied samples: (A) Pyrite framboids in sample A-7; (B) Framboidal pyrite made up of uniform microcrystals in sample A-8; (C) Pyrite framboids in sample A-11; and (D) Pyrite framboids with a tail in sample A-22.

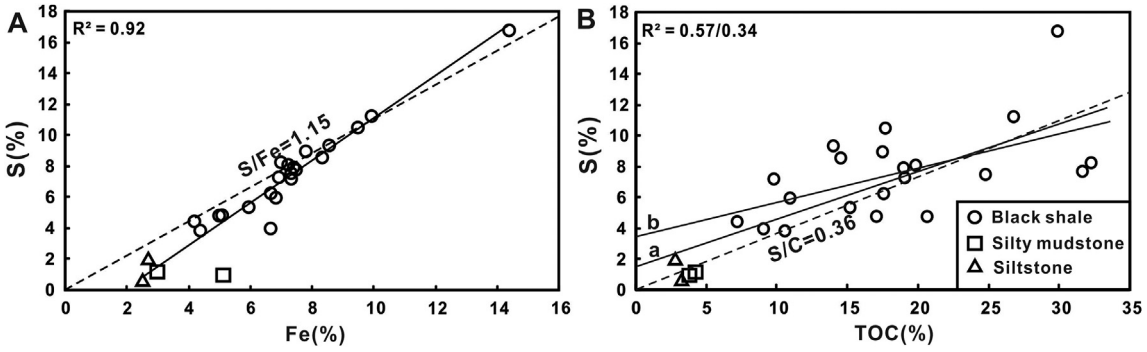

Fig. 8. The relationship of iron and organic carbon to the sulfur content of the TICBS.

organic matter enrichment (e.g. Böning et al., 2012; Wei et al., 2012; Yan et al., 2015). However, we need to certify that the TOC above refers to the organic matter produced by algae organisms (primary productivity) before compare (Pedersen and Calvert, 1990). In fact, previous research had certified that the organic matter of the Chang7 black shales was mainly algae coming from primary productivity. For instance, the kerogen of the Chang7 black shales was consisted of average value being 91.08% amorphous liptinite and less than 10% the vitrinite (terrestrial debris) (Yang and Zhang, 2005; Kong, 2007); the kerogen's $\delta^{13}C$ of the Chang7 black shales ranges from −30‰ to −28‰ (Guo et al., 2014; Ji et al., 2007), which is in the range of algae (Meyers, 1994); the abundance of cyanobacteria fossils in the Chang7 black shales is closely related to the organic carbon contents of black shales (Ji et al., 2012). Therefore, TOC in our paper can be compared with the productivity proxies and the details are as follows.

Phosphorus is considered as an important nutrient which limits biological growth (Ingall et al., 1993; Vink et al., 1997; Slomp et al., 2004). The distributions of phosphorous (P) in sediments are often linked to supply of organic matter, possibly resulting from a high productivity, which makes P an important indicator for biological productivity (Schmitz et al., 1997). The P/Al in the black shales are higher with a larger range, while in siltstones (silty mudstones), it is lower with a smaller range. As a whole, the P/Al shows a rapid and frequent change (Fig. 4). These data suggest that a significant change possibly occurred in primary productivity when the TICBS were deposited. In addition, the P/Al and TOC have nearly the same profile trends, indicating that the primary productivity is likely to exert an important influence on the enrichment of organic matter.

Nickel (Ni) and copper (Cu) are predominantly delivered to the sediments in association with the OM (organometallic complexes), so the contents of sedimentary organic matter are often proportional to Ni and Cu (Tribovillard et al., 2006). Consequently, organic matter may be partially or completely degraded after deposition, whereas the Ni and Cu released by the organic matter are trapped by pyrite and are retained within the sediments (Huerta-Diaz and

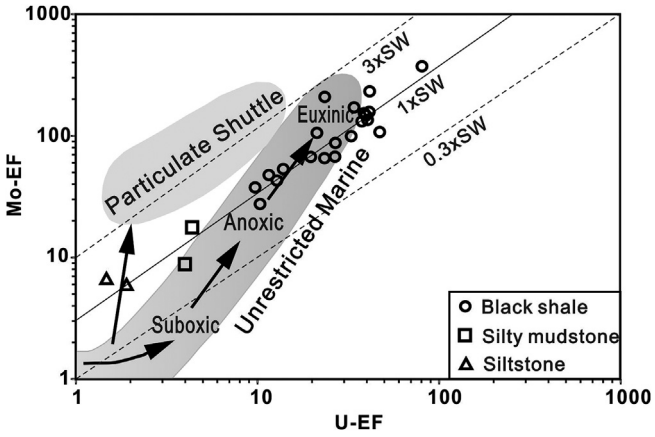

Fig. 9. U_{EF} versus Mo_{EF} for the TICBS. The lines show Mo/U molar ratios equal to the seawater value (SW) and to the fractions thereof (3 × SW, 0.3 × SW). The pattern of U_{EF} and Mo_{EF} are compared to the model proposed by Algeo and Tribovillard (2009).

Morse, 1992; Algeo and Maynard, 2004; Nameroff et al., 2004; Piper and Perkins, 2004); hence, the Ni and Cu can be used as indicators for paleoproductivity (Tribovillard et al., 2006). The average Cu/Al and Ni/Al of the Peru upwelling area (Productive area) are 8.00×10^{-4} and 7.30×10^{-4}, and their background values with TOC being zero are 1.8×10^{-4} or 2.7×10^{-4} and 0.7×10^{-4} or 1.4×10^{-4}, respectively (Böning et al., 2012). The Cu/Al of the black shales are much higher than those of Peru, and Ni/Al are slightly higher than those of Peru (Fig. 4), whilst the background values with TOC being zero (1.14×10^{-4} and 2.63×10^{-4}, respectively) (Fig. 10D and C) are similar to the Peru area. Therefore, the paleoproductivity of the black shales was possibly very high. In addition, the coincidence of an increased abundance of total organic carbon (TOC) with increased Cu/Al, Ni/Al, and P/Al (Fig. 4) indicates that the organic matter accumulation in the TICBS was mainly controlled by increased primary productivity.

The barite accumulation rate shows a positive correlation with primary productivity in the marine sediments (Dymond et al., 1992; Dymond and Collier, 1996; Paytan, 1996; Paytan and Griffith, 2007). Therefore, the Ba/Al ratio can be used in order to quantitatively evaluate the paleoproductivity (Dean et al., 1997). However, when the primary productivity is very high, a strong BSR may cause barite dissolution and Ba loss in the sediments, thus reducing the reliability of the Ba/Al proxy (Van Os et al., 1991; Torres et al., 1996; Van Santvoort et al., 1996; Tribovillard et al., 2006). The profile variations of Ba/Al are very different from the Cu/Al, Ni/Al, P/Al and TOC contents, with Ba/Al values of most black shale samples lower than the values of the siltstone (silty mudstone) samples (Fig. 4). Combined with the characteristics of the abundant reduced sulfur and pyritic sulfur isotopes in the black shales, these data indicate that the intense BSR possibly led to barite dissolution in the sediments and transformed the original Ba content in shales. Thus, the Ba/Al in this profile cannot reflect the true paleoproductivity.

4.4. Clastic influx

Clastic influx is indicative of the fact that the diluents and absorbents of organic matter may directly affect the content of organic matter in the sediments (Ibach, 1982; Rimmer, 2004), and thus indirectly affect the burial rate and bacteria degradation efficiency of the organic matter (Canfield, 1994). Al in sediments is all from clay, feldspar and other aluminum silicate minerals, while Ti is partly from clay minerals, and partly from silt-sized gains of heavy minerals (such as ilmenite, sphene, and augite) (Rimmer, 2004). Thus, the Ti/Al can be used as a reliable indicator of the siliciclastic grain size (Bertrand et al., 1996). As the grains of sediment increase with the sedimentation rates, higher Ti/Al represent the larger grains and faster sedimentation rates (Murphy et al., 2000).

The Ti/Al of the TICBS in the profile show a relatively steady trend (Fig. 3). The Ti/Al of the siltstones and silty mudstones are slightly higher than those of the black shales, but all of them are lower than the anoxic marine sediments (e.g., Longmaxi Formation in South China in which the Ti/Al is 0.058; Yan et al., 2015). Meanwhile, based on the age model which was constructed using the zircon U-Pb age of tuff and strata thickness (Yang and Deng, 2013), and Milankovitch cycle (Earth orbital cycle) (Yuan et al., 2016a), the average sedimentation rate of the Chang7 shales is 1.5 cm/kyr (5 cm/kyr by taking into account the compaction rate of the mudstone (70%, Chen and Wan, 1984)) and 1.35 cm/kyr, respectively, which are between the open marine settings (<1 cm/kyr, Loutit et al., 1988; Katz, 2005) and the strongly limited marine basins (eg. Black sea Unit II, 7.8–21.4 cm/kyr, Arthur and Dean, 1998), so the information deduced by Ti/Al is nearly consistent with the sedimentation rate here, namely, the sedimentation rate may have been lower when the TICBS were deposited. In addition, the Ti/Al and TOC data show a very weak negative correlation ($R^2 = 0.02$) (Fig. 10E) suggesting that the enrichment of the organic matter possibly has no relationship with the detrital input/sedimentation rate. Therefore, the burial of organic matter in the TICBS was not simply a function of clastic starvation or the increased surface area for organic matter adsorption associated with finer grains.

4.5. The mechanism of organic matter accumulation

The factors controlling organic matter enrichment include surficial primary productivity (Pedersen and Calvert, 1990; Caplan and Bustin, 1999), sedimentation rate (clastic influx) (Murphy et al., 2000; Sageman et al., 2003) and redox conditions (Demaison and Moore, 1980; Mort et al., 2007). The clastic influx indicator (Ti/Al) of the TICBS has a relatively steady trend (Fig. 3) and has no correlation with the TOC contents ($R^2 = 0.02$) (Fig. 10 E) suggesting that the change of clastic influx was not the main factor controlling the enrichment of the organic matter in the TICBS. The redox (U/Th) and productivity (Cu/Al, Ni/Al, and P/Al) indicators and TOC contents show a similar trend (Fig. 4), as well as the U/Th, Cu/Al, and Ni/Al with TOC have good positive correlations ($R^2 = 0.59$, 0.62 and 0.56, respectively) (Fig. 10). This indicates that the anoxic conditions and high productivity joined together to enhance preservation and accumulation of sedimentary organic matter, resulting in the deposition of the TICBS.

However, which factor on Earth is more important? Schoepfer et al. (2015) proposed that the covariant relations of TOC vs. P and TOC vs. Ba can be used to distinguish the relative importance between the redox conditions and productivity levels in the process of organic matter enrichment. When the redox conditions are more critical, in reducing conditions, TOC tends to save, while P and Ba prefer to activate and are lost as their adsorption carriers (ferromanganese hydroxide) are reduced and dissolved. In oxidizing conditions, the TOC is easily consumed by oxygen, while P and Ba tend to be buried and deposited. Therefore, either in oxidizing or reducing conditions, the TOC vs. P and TOC vs. Ba always show an anti-covariant relationship (Tyson, 2005). When primary productivity is more important, the output of organic matter in surface water is the main factor controlling for the TOC, P, and Ba in sediments. The redox conditions will generally not affect the strong positive correlation of TOC vs. P and TOC vs. Ba (Tyson, 2005); however, the correlation of TOC vs. Ba may possibly be lost as a result of the intense sulfate reduction (Reichart et al.,

1997; Muñoz et al., 2012).

The P/Al and TOC of the TICBS show a good positive correlation (Fig. 10A solid line a, $R^2 = 0.71$, excluding the sample A-24), and the black shales (excluding siltstones and silty mudstones) exhibits a better positive correlation ($R^2 = 0.81$, Fig. 10A solid line b), suggesting that the organic matter enrichment in the TICBS may have been predominantly derived by primary productivity. However, the Ba/Al and TOC do not show any correlation ($R^2 = 0.02$, Fig. 10B), which may have been related to the intense sulfate reduction, possibly resulting in by high productivity (see section 4.3). Therefore, we suggest that the primary productivity was more important in organic matter enrichment in the TICBS, and the anoxic to sulfidic conditions in the lake may have been the result of the intense degradation of organic matter.

The level of primary productivity is largely controlled by nutrient availability in any sedimentary basins (Katz, 1995). For one thing, as the marine incursion events possibly occurred when the TICBS were deposited, so the nutrients were possible seawater-sourced and entered the basin through lateral advection when the shales deposited. That is to say, surface waters flow oceanward and deep waters cratonward while nutrients are brought in with the laterally advected deep waters. Then, they recycled between the surface and deep layers of the basin, such as the Permian Phosphoria Formation on the western margin of North America (Stephens and Carroll, 1999), as well as the Late Pennsylvanian Midcontinent Sea of North America (Algeo et al., 2008a; Algeo and Heckel, 2008). For another thing, experimental research shows that the volcanic ashes can release large amounts of major and trace nutrients such as P, Si, Fe, Zn, Mn, Ni, Co, and Cu, etc. in 1–2 h, thus creating favorable conditions for a large-scale phytoplankton blooms (Frogner et al., 2001). Field observations have also confirmed the rapid blooms of phytoplankton in lakes and oceans after deposition of ash and aerosols. For example, the eruption of Mount St. Helens in Washington on May 18, 1980, was followed by a proliferation of phytoplankton in its nearby lakes (Smith and White, 1985); In August 2008, when the Kasatochi volcano of the Aleutian Islands erupted, volcanic ashes were deposited over a large area, with satellite observations showing a massive increase in the biological chlorophyll within the Northeast Pacific region (Hamme et al., 2010). It is noteworthy that there are abundant volcanic ash layers in the TICBS and overlying those volcanic layers, phosphate nodules were also found (Fig. 2B and D), which could be possibly related to high productivity. Furthermore, the P/Al and TOC also show a strong positive correlation. All these data suggest that the increase of paleoproductivity in the Chang7 period was likely driven by lateral advection of seawater-freshwater or the deposition of volcanic ash supplying abundant nutrients.

5. Conclusions

Sedimentary petrographic and geochemical data in conjunction with the published paleontological and sedimentation rate data were used to reveal the depositional environments and processes of organic matter accumulation in the black shales from the

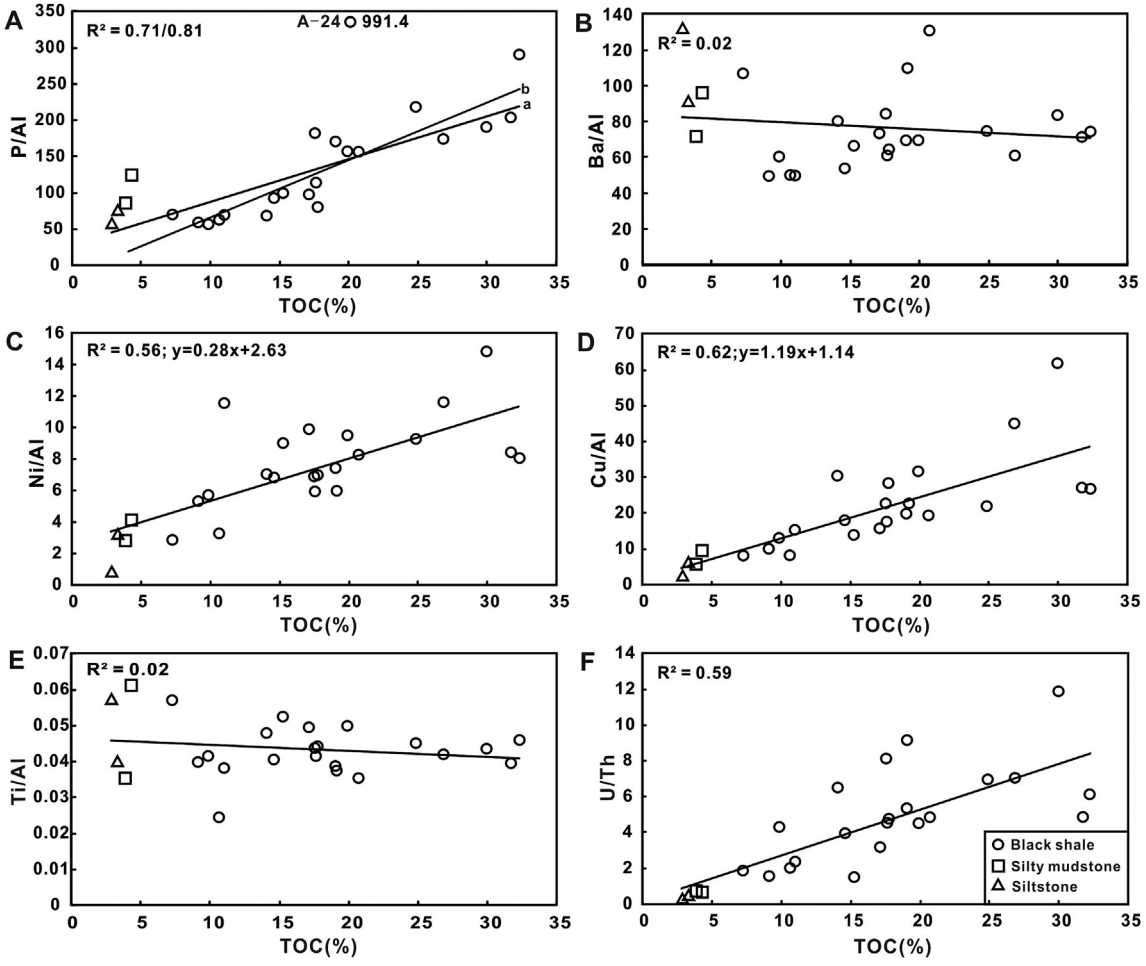

Fig. 10. The relationship of TOC to P/Al (× 10^{-4}), Ba/Al (× 10^{-4}), Ni/Al (× 10^{-4}), Cu/Al (× 10^{-4}), Ti/Al, and U/Th of the TICBS.

Yanchang Formation of the Ordos Basin. Our findings are summarized as follows:

(1) The typical intervals of the Chang7 black shales were deposited in a lacustrine environment possibly intruded by seawater.
(2) The typical intervals of the Chang7 black shales are mainly composed of black shale intercalated with thin siltstone (silty mudstone) caused by the turbidity currents and laminated tuff from volcanism.
(3) The typical intervals of the Chang7 black shales were mainly deposited under anoxic to sulfidic bottom water conditions, which were interrupted by the oxygen-containing turbidity currents.
(4) Organic matter enrichment was controlled by primary productivity, which was possibly increased in unison with an influx of nutrients from seawater or volcanic eruptions. This along with the anoxic to sulfidic water mass, which was possibly caused by the intense degradation of the organic matter during early diagenesis of the accumulated organic matter, results in enhanced organic matter accumulation and preservation in the typical intervals of the Chang7 black shales.

Acknowledgements

We would like to thank Liang Qi from the Institute of Geochemistry, Chinese Academy of Sciences, for the major and trace metals analysis. This research was supported by the National Natural Science Foundation of China (41321002 and 41272144) and the scientific and technological project B of the strategic precursor, the Chinese Academy of Sciences (XDB10000000). We would like to extend thank you for improving the grammer of the manuscript by Prof. Harunur Rashid, the insightful comments and suggestions by Thomas Algeo and an anonymous reviewer, and Editor-in-chief Andrew Bell is highly acknowledged. This paper is Contribution No. IS-2394 from GIGCAS.

References

Algeo, T.J., Heckel, P.H., 2008. The Late Pennsylvanian midcontinent sea of North America: a review. Palaeogeogr. Palaeoclimatol. Palaeoecol. 268, 205–221.
Algeo, T.J., Heckel, P.H., Maynard, J.B., Blakey, R.C., Rowe, H., 2008a. Modern and Ancient Epeiric Seas and the Super-estuarine Circulation Model of Marine Anoxia. Dynamics of Epeiric Seas: Sedimentological, Paleontological and Geochemical Perspectives. Geological Association Canada Special Publication, pp. 7–38.
Algeo, T.J., Luo, G.M., Song, H.Y., Lyons, T.W., Canfield, D.C., 2015. Reconstruction of secular variation in seawater sulfate concentrations. Biogeosciences 12, 2131–2151.
Algeo, T.J., Maynard, J.B., 2004. Trace-element behavior and redox facies in core shales of Upper Pennsylvanian Kansas-type cyclothems. Chem. Geol. 206, 289–318.
Algeo, T.J., Maynard, J.B., 2008. Trace-metal covariation as a guide to water-mass conditions in ancient anoxic marine environments. Geosphere 4, 872–887.
Algeo, T.J., Rowe, H., Hower, J.C., Schwark, L., Herrmann, A., Heckel, P., 2008b. Changes in ocean denitrification during Late Carboniferous glacial-interglacial cycles. Nat. Geosci. 1, 709–714 (supplementary information).
Algeo, T.J., Tribovillard, N., 2009. Environmental analysis of paleoceanographic systems based on molybdenum–uranium covariation. Chem. Geol. 268, 211–225.
Arthur, M.A., Dean, W.E., 1998. Organic-matter production and preservation and evolution of anoxia in the Holocene Black Sea. Paleoceanography 13, 395–411.
Arthur, M.A., Sageman, B.B., 1994. Marine shales: depositional mechanisms and environments of ancient deposits. Annu. Rev. Earth Planet. Sci. 22, 499–551.
Böning, P., Fröllje, H., Beck, M., Schnetger, B., Brumsack, H.-J., 2012. Underestimation of the authigenic fraction of Cu and Ni in organic-rich sediments. Mar. Geol. 323, 24–28.
Berner, R.A., 1984. Sedimentary pyrite formation: an update. Geochimica Cosmochimica Acta 48, 605–615.
Berner, R.A., Raiswell, R., 1984. C/S method for distinguishing freshwater from marine sedimentary rocks. Geology 12, 365–368.
Bertrand, P., Shimmield, G., Martinez, P., Grousset, F., Jorissen, F., Paterne, M., Pujol, C., Bouloubassi, I., Menard, P.B., Peypouquet, J.-P., 1996. The glacial ocean productivity hypothesis: the importance of regional temporal and spatial studies. Mar. Geol. 130, 1–9.
Boschetti, T., Cortecchi, G., Toscani, L., Iacumin, P., 2011. Sulfur and oxygen isotope compositions of Upper Triassic sulfates from Northern Apennines (Italy): palaeogeographic and hidrogeochemical implications. Geol. Acta 9, 129–147.
Burdige, D.J., 2007. Preservation of organic matter in marine sediments: controls, mechanisms, and an imbalance in sediment organic carbon budgets? Chem. Rev. 107, 467–485.
Canfield, D.E., 1994. Factors influencing organic carbon preservation in marine sediments. Chem. Geol. 114, 315–329.
Canfield, D.E., 2001. Biogeochemistry of sulfur isotopes. In: Valley, J.W., Cole, D.R. (Eds.), Reviews in Mineralogy and Geochemistry: Stable Isotope Geochemistry, 43. Mineralogical Society of America, pp. 607–636.
Canfield, D.E., Raiswell, R., Westrich, J.T., Reaves, C.M., Berner, R.A., 1986. The use of chromium reduction in the analysis of reduced inorganic sulfur in sediments and shales. Chem. Geol. 54, 149–155.
Caplan, M.L., Bustin, R.M., 1999. Palaeoceanographic controls on geochemical characteristics of organic-rich Exshaw mudrocks: role of enhanced primary production. Org. Geochem. 30, 161–188.
Chambers, L.A., 1982. Sulfur isotope study of a modern intertidal environment, and the interpretation of ancient sulfides. Geochimica Cosmochimica Acta 46, 721–728.
Chen, Z.M., Wan, L.G., 1984. A calculating method on the fossil thickness of stratigraphy. Oil Gas Geol. 5, 47–54 (in Chinese with English abstract).
Dean, W.E., Arthur, M.A., 1989. Iron-sulfur-carbon relationships in organic-carbon-rich sequences I: cretaceous western interior seaway. Am. J. Sci. 289, 708–743.
Dean, W.E., Gardner, J.V., Piper, D.Z., 1997. Inorganic geochemical indicators of glacial-interglacial changes in productivity and anoxia on the California continental margin. Geochimica Cosmochimica Acta 61, 4507–4518.
Demaison, G.T., Moore, G.T., 1980. Anoxic environments and oil source bed genesis. Org. Geochem. 2, 9–31.
Deng, X.Q., Lin, F.X., Liu, X.Y., Pang, J.L., Lv, J.W., Li, S.X., Liu, X., 2008. Discussion on relationship between sedimentary evolution of the triassic Yanchang Formation and the early indosinian movement in Ordos basin. J. Palaeogeogr. 10, 159–166 (in Chinese with English abstract).
Dymond, J., Collier, R., 1996. Particulate barium fluxes and their relationships to biological productivity. Deep Sea Res. Part II Top. Stud. Oceanogr. 43, 1283–1308.
Dymond, J., Suess, E., Lyle, M., 1992. Barium in deep-sea sediment: a geochemical proxy for paleoproductivity. Paleoceanography 7, 163–181.
Feng, P.J., Li, W.H., Ou, Y.Z.J., 2012. Sedimentary characters and geological implication of turbidite of the Chang 6 and Chang 7 intervals of upper triassic Yanchang Formation in Huangling area, Ordos basin. J. Palaeogeogr. 14, 295–302 (in Chinese with English abstract).
Frogner, P., Gíslason, S.R., Óskarsson, N., 2001. Fertilizing potential of volcanic ash in ocean surface water. Geology 29, 487–490.
Fu, X.Z., Wang, J., Chen, W.B., Feng, X.L., Wang, D., Song, C.Y., Zeng, S.Q., 2015. Organic accumulation in lacustrine rift basin: constraints from mineralogical and multiple geochemical proxies. Int. J. Earth Sci. 104, 495–511.
Guo, H.J., Jia, W.L., Peng, P.A., Lei, Y.H., Luo, X.R., Cheng, M., Wang, X.Z., Zhang, L.X., Jiang, C.F., 2014. The organic geochemistry, mineralogy and methane sorption of lacustrine shales from the Upper Triassic Yanchang Formation, Ordos Basin, China. Mar. Petroleum Geol. 57, 509–520.
Habicht, K.S., Canfield, D.E., 1996. Sulphur isotope fractionation in modern microbial mats and the evolution of the sulphur cycle. Nature 382, 342–343.
Habicht, K.S., Canfield, D.E., 1997. Sulfur isotope fractionation during bacterial sulfate reduction in organic-rich sediments. Geochimica Cosmochimica Acta 61, 5351–5361.
Hamme, R.C., Webley, P.W., Crawford, W.R., Whitney, F.A., DeGrandpre, M.D., Emerson, S.R., Eriksen, C.C., Giesbrecht, K.E., Gower, J.F.R., Kavanaugh, M.T., Pena, M.A., Sabine, C.L., Batten, S.D., Coogan, L.A., Grundle, D.S., Lockwood, D., 2010. Volcanic ash fuels anomalous plankton bloom in subarctic northeast Pacific. Geophys. Res. Lett. 37, 470–479.
Hay, W.W., 1995. Paleoceanography of marine organic-carbon-rich sediments. In: Huc, A.-Y. (Ed.), Paleogeography, Paleoclimate, and Source Rocks, 40. American Association of Petroleum Geologists, Studies in Geology, pp. 21–59.
Hedges, J.I., Keil, R.G., 1995. Sedimentary organic matter preservation: an assessment and speculative synthesis. Mar. Chem. 49, 81–115.
Hofmann, P., Ricken, W., Schwark, L., Leythaeuser, D., 2000. Carbon-sulfur-iron relationships and $\delta^{13}C$ of organic matter for late Albian sedimentary rocks from the North Atlantic Ocean: paleoceanographic implications. Palaeogeography 163, 97–113.
Huang, Y.J., Yang, G.S., Gu, J., Wang, P.K., Huang, Q.H., Feng, Z.H., Feng, L.J., 2013. Marine incursion events in the Late Cretaceous Songliao Basin: constraints from sulfur geochemistry records. Palaeogeogr. Palaeoclimatol. Palaeoecol. 385, 152–161.
Huerta-Diaz, M.A., Morse, J.W., 1992. Pyritization of trace metals in anoxic marine sediments. Geochimica Cosmochimica Acta 56, 2681–2702.
Ibach, L.E.J., 1982. Relationship between sedimentation rate and total organic carbon content in ancient marine sediments. AAPG Bull. 66, 170–188.
Ingall, E.D., Bustin, R.M., Cappellen, P.V., 1993. Influence of water column anoxia on the burial and preservation of carbon and phosphorus in marine shales. Geochimica Cosmochimica Acta 57, 303–316.

Ji, L.M., Wang, S.F., Xu, J.L., 2006. Acritarch Assemblage in Yanchang Formaton in Eastern Gansu Province and its Environmental Implications. Earth Science-Journal of China University of Geosciences 31, pp. 798–806 (in Chinese with English abstract).
Ji, L.M., Wu, T., Li, L.T., 2007. Geochemical characteristics of kerogen in Yanchang Formation source rocks, Xifeng area, Ordos basin. Petroleum Explor. Dev. 34, 424–428 (in Chinese with English abstract).
Ji, L.M., Xu, J.L., Song, Z.G., 2012. Lacustrine cyanobacteria from the Yanchang Formation in Ordos basin and its implication of oil source. Acta Micropalaeontologica Sin. 3, 270–281 (in Chinese with English abstract).
Kaplan, I.R., Rittenberg, S.C., 1964. Microbiological fractionation of sulphur isotopes. J. General Microbiol. 34, 195–212.
Katz, B.J., 1995. Factors controlling the development of lacustrine petroleum source rocks—an update. In: Huc, A.-Y. (Ed.), Paleogeography, Paleoclimate, and Source Rocks, vol. 40. American Association of Petroleum Geologists, Studies in Geology, pp. 61–79.
Katz, B.J., 2005. Controlling factors on source rock development-a review of productivity, preservation, and sedimentation rate. Soc. Sediment. Geol. 82, 7–16.
Kimura, H., Watanabe, Y., 2001. Oceanic anoxia at the Precambrian-Cambrian boundary. Geology 29, 995.
Kong, Q.F., 2007. The organic maceral characteristic of Yanchang source rock in Ordos Basin. Xinjiang Pet. Geol. 28, 163–166 (in Chinese with English abstract).
Lash, G.G., Blood, D.R., 2014. Organic matter accumulation, redox, and diagenetic history of the Marcellus Formation, southwestern Pennsylvania, Appalachian basin. Mar. Petroleum Geol. 57, 244–263.
Leventhal, J.S., 1983. An interpretation of carbon and sulfur relationships in Black Sea sediments as indicators of environments of deposition. Geochimica Cosmochimica Acta 47, 133–137.
Leventhal, J.S., 1987. C and S relationships in Devonian shales from the Appalachian basin as an indicator of environment of deposition. Am. J. Sci. 287, 33–49.
Liu, G.B., Zhu, Z.X., Zhang, X.L., Ai, F., 1999. A coelacanthid fossil from Huachi area, Gansu province. Geol. J. China Univ. 4, 474–480 (in Chinese with English abstract).
Liu, S., 1998. The coupling mechanism of basin and orogen in the western Ordos Basin and adjacent regions of China. J. Asian Earth Sci. 16, 369–383.
Liu, S., Yang, S., 2000. Upper Triassic–Jurassic sequence stratigraphy and its structural controls in the western Ordos Basin, China. Basin Res. 12, 1–18.
Loutit, T.S., Hardenbol, J., Vail, P.R., Baum, G.R., 1988. Condensed sections: the key to age determination and correlation of continental margin sequences. SEPM 42, 183–213.
Luo, M., Algeo, T.J., Tong, H.P., Gieskes, J., Chen, L.Y., Shi, X.F., Chen, D.F., 2017. More reducing bottom-water redox conditions during the Last Glacial Maximum in the southern Challenger Deep (Mariana Trench, western Pacific) driven by enhanced productivity. Deep Sea Res. Part II Top. Stud. Oceanogr. http://dx.doi.org/10.1016/j.dsr2.2017.01.006.
Lyons, T.W., Berner, R.A., 1992. Carbon-sulfur-iron systematics of the uppermost deep-water sediments of the Black Sea. Chem. Geol. 99, 1–27.
Meyers, P.A., 1994. Preservation of elemental and isotopic source identification of sedimentary organic matter. Chem. Geol. 114, 289–302.
McLennan, S., 1989. Rare earth elements in sedimentary rocks; influence of provenance and sedimentary processes. Rev. Mineralogy Geochem. 21, 169–200.
Mort, H., Jacquat, O., Adatte, T., Steinmann, P., Föllmi, K., Matera, V., Berner, Z., Stüben, D., 2007. The Cenomanian/Turonian anoxic event at the Bonarelli Level in Italy and Spain: enhanced productivity and/or better preservation? Cretac. Res. 28, 597–612.
Muñoz, P., Dezileau, L., Cardenas, L., Sellanes, J., Lange, C.B., Inostroza, J., Muratli, J., Salamanca, M.A., 2012. Geochemistry of trace metals in shelf sediments affected by seasonal and permanent low oxygen conditions off central Chile, SE Pacific (~36°S). Cont. Shelf Res. 33, 51–68.
Murphy, A.E., Sageman, B.B., Hollander, D.J., Lyons, T.W., Brett, C.E., 2000. Black shale deposition and faunal overturn in the Devonian Appalachian Basin: clastic starvation, seasonal water-column mixing, and efficient biolimiting nutrient recycling. Paleoceanography 15, 280–291.
Nameroff, T.J., Calvert, S.E., Murray, J.W., 2004. Glacial-interglacial variability in the eastern tropical North Pacific oxygen minimum zone recorded by redox-sensitive trace metals. Paleoceanography 19, 373–394.
Parrish, J.T., 1995. Paleogeography of C org-rich rocks and the preservation versus production controversy. In: Huc, A.Y. (Ed.), Paleogeography, Paleoclimate, and Source Rocks, vol. 40. American Association of Petroleum Geologists, Studies in Geology, pp. 1–20.
Paytan, A., 1996. Glacial to interglacial fluctuations in productivity in the Equatorial Pacific as indicated by marine barite. Science 274, 1355–1357.
Paytan, A., Griffith, E.M., 2007. Marine barite: recorder of variations in ocean export productivity. Deep Sea Res. Part II Top. Stud. Oceanogr. 54, 687–705.
Pedersen, T.F., Calvert, S.E., 1990. Anoxia vs. productivity: what controls the formation of organic-carbon-rich sediments and sedimentary Rocks? AAPG Bull. 74, 454–466.
Piper, D.Z., Perkins, R.B., 2004. A modern vs. Permian black shale-the hydrography, primary productivity, and water-column chemistry of deposition. Chem. Geol. 206, 177–197.
Qi, L., Zhou, M.F., Malpas, J., Sun, M., 2005. Determination of rare earth elements and Y in ultramafic rocks by ICP-MS after preconcentration using $Fe(OH)_3$ and $Mg(OH)_2$ coprecipitation. Geostand. Geoanalytical Res. 29, 131–141.
Qiu, D.Z., Xie, Y., Li, X.Q., Huang, F.X., 2009a. Geological characteristics of lithofacies paleogeography and hydrocarbon accumulation in Asian tethyan tectonic domain. Mar. Orig. Pet. Geol. 14, 41–51.
Qiu, X.W., 2011. Characteristics and Dynamic Settings of Yanchang Period Hydrocarbon-rich Depression in Ordos Basin (PhD Dissertation). Northwest University, Xi'an (in Chinese with English abstract).
Qiu, X.W., Liu, C.Y., Li, Y.H., Mao, G.Z., Wang, J.Q., 2009b. Distribution characteristics and geological significances of tuff interlayers in Yanchang formation of Ordos basin, China. Acta Sedimentol. Sin. 27, 1138–1146 (in Chinese with English abstract).
Qiu, X.W., Liu, C.Y., Mao, G.Z., Deng, Y., Wang, F.F., 2010. Enrichment feature of thorium element in tuff interlayers of Upper Triassic Yanchang formation in Ordos basin, China. Geol. Bull. China 29, 1185–1191 (in Chinese with English abstract).
Qiu, X.W., Liu, C.Y., Mao, G.Z., Deng, Y., Wang, F.F., Wang, J.Q., 2014. Major, trace and platinum-group element geochemistry of the Upper Triassic nonmarine hot shales in the Ordos basin, Central China. Appl. Geochem. 53, 42–52.
Raiswell, R., Berner, R.A., 1985. Pyrite formation in euxinic and semi-euxinic sediments. Am. J. Sci. 285, 710–724.
Raiswell, R., Buckley, F., Berner, R.A., Anderson, T.F., 1988. Degree of pyritization of iron as a paleoenvironmental indicator of bottom-water oxygenation. J. Sediment. Res. 58, 812–819.
Reichart, G.J., Dulk, M.D., Visser, H.J., Weijden, C.H.V.D., Zachariasse, W.J., 1997. A 225 kyr record of dust supply, paleoproductivity and the oxygen minimum zone from the Murray Ridge (northern Arabian Sea). Palaeogeogr. Palaeoclimatol. Palaeoecol. 134, 149–169.
Rimmer, S.M., 2004. Geochemical paleoredox indicators in devonian-mississippian black shales, central Appalachian Basin (USA). Chem. Geol. 206, 373–391.
Rimmer, S.M., Thompson, J.A., Goodnight, S.A., Robl, T.L., 2004. Multiple controls on the preservation of organic matter in Devonian–Mississippian marine black shales: geochemical and petrographic evidence. Palaeogeogr. Palaeoclimatol. Palaeoecol. 215, 125–154.
Riquier, L., Tribovillard, N., Averbuch, O., Devleeschouwer, X., Riboulleau, A., 2006. The Late Frasnian Kellwasser horizons of the Harz Mountains (Germany): two oxygen-deficient periods resulting from different mechanisms. Chem. Geol. 233, 137–155.
Sageman, B.B., Murphy, A.E., Werne, J.P., Ver Straeten, C.A., Hollander, D.J., Lyons, T.W., 2003. A tale of shales: the relative roles of production, decomposition, and dilution in the accumulation of organic-rich strata, Middle-Upper Devonian, Appalachian basin. Chem. Geol. 195, 229–273.
Schmitz, B., Charisi, S.D., Thompson, E.I., Speijer, R.P., 1997. Barium, SiO_2 (excess), and P_2O_5 as proxies of biological productivity in the Middle East during the Palaeocene and the latest Palaeocene benthic extinction event. Terra nova. 9, 95–99.
Schoepfer, S.D., Shen, J., Wei, H., Tyson, R.V., Ingall, E., Algeo, T.J., 2015. Total organic carbon, organic phosphorus, and biogenic barium fluxes as proxies for paleomarine productivity. Earth-Science Rev. 149, 23–52.
Schwarcz, H.P., Burnie, S.W., 1973. Influence of sedimentary environments on sulfur isotope ratios in clastic rocks: a review. Miner. Deposita 8, 264–277.
Slomp, C.P., Thomson, J., Lange, G.J.D., 2004. Controls on phosphorus regeneration and burial during formation of eastern Mediterranean sapropels. Mar. Geol. 203, 141–159.
Smith, M.A., White, M.J., 1985. Observations on lakes near Mount St. Helens: phytoplankton. Arch. Fuer Hydrobiol. 104, 345–362.
Stephens, N.P., Carroll, A.R., 1999. Salinity stratification in the Permian Phosphoria sea: a proposed paleoceanographic model. Geology 27, 899–902.
Strauss, H., 1997. The isotopic composition of sedimentary sulfur through time. Palaeogeogr. Palaeoclimatol. Palaeoecol. 132, 97–118.
Su, D.Z., 1984. A new palaeoniscoid fish from the Yanchang Group of North Shaanxi and its biostratigraphic significance. Vertebr. Palasiat. 22, 14–21 (in Chinese with English abstract).
Thompson, C.K., Kah, L.C., 2012. Sulfur isotope evidence for widespread euxinia and a fluctuating oxycline in Early to Middle Ordovician greenhouse oceans. Palaeogeogr. Palaeoclimatol. Palaeoecol. 313, 189–214.
Torres, M.E., Brumsack, H.J., Bohrman, G., Emeis, K.C., 1996. Barite front in continental margin sediments: a new look at barium remobilization in the zone of sulfate reduction and formation of heavy barites in diagenetic fronts. Chem. Geol. 127, 125–139.
Tribovillard, N., Algeo, T.J., Baudin, F., Riboulleau, A., 2012. Analysis of marine environmental conditions based on molybdenum-uranium covariation–Applications to Mesozoic paleoceanography. Chem. Geol. 324, 46–58.
Tribovillard, N., Algeo, T.J., Lyons, T., Riboulleau, A., 2006. Trace metals as paleoredox and paleoproductivity proxies: an update. Chem. Geol. 232, 12–32.
Tyson, R.V., 2005. The "productivity versus preservation" controversy: cause, flaws, and resolution. Spec. Publ. 82, 17–33.
Van Os, B.J.H., Middelburg, J.J., de Lange, G.J., 1991. Possible diagenetic mobilization of barium in sapropelic sediments from the eastern Mediterranean. Mar. Geol. 100, 125–136.
Van Santvoort, P.J.M., de Lange, G.J., Thomson, J., Cussen, H., Wilson, T.R.S., Krom, M.D., Ströhle, K., 1996. Active postdepositional oxidation of the most recent sapropel (S1) in sediments of the eastern Mediterranean Sea. Geochimica Cosmochimica Acta 60, 4007–4024.
Vink, S., Chambers, R.M., Smith, S.V., 1997. Distribution of phosphorus in sediments from tomales bay, California. Mar. Geol. 139, 157–179.
Watanabe, T., Naraoka, H., Nishimura, M., Kawai, T., 2004. Biological and environmental changes in lake baikal during the late quaternary inferred from carbon, nitrogen and sulfur isotopes. Earth Planet. Sci. Lett. 222, 285–299.

Wei, H., Chen, D., Wang, J., Yu, H., Tucker, M.E., 2012. Organic accumulation in the lower Chihsia Formation (Middle Permian) of South China: constraints from pyrite morphology and multiple geochemical proxies. Palaeogeogr. Palaeoclimatol. Palaeoecol. 353, 73–86.
Wignall, P.B., Twitchett, R.J., 1996. Oceanic anoxia and the End Permian mass extinction. Science 272, 1155–1158.
Wignall, P.B., Newton, R., 1998. Pyrite framboid diameter as a measure of oxygen deficiency in ancient mudrocks. Am. J. Sci. 298, 537–552.
Wilkin, R.T., Barnes, H.L., 1996. Pyrite formation by reactions of iron monosulfides with dissolved inorganic and organic sulfur species. Geochimica Cosmochimica Acta 60, 4167–4179.
Wilkin, R.T., Barnes, H.L., 1997. Formation processes of framboidal pyrite. Geochimica Cosmochimica Acta 61, 323–339.
Xu, W., Wang, W.Y., Zhang, Q., 2003. Primary discussion on the recent development of the geological theory in China. China Pet. Explor. 8, 18–24 (in Chinese with English abstract).
Yan, D., Wang, H., Fu, Q., Chen, Z., He, J., Gao, Z., 2015. Geochemical characteristics in the Longmaxi Formation (early silurian) of South China: implications for organic matter accumulation. Mar. Petroleum Geol. 65, 290–301.
Yang, H., Deng, X.Q., 2013. Deposition of Yanchang Formation deep-water sandstone under the control of tectonic events, Ordos Basin. Petroleum Explor. Dev. 40, 513–520 (in Chinese with English abstract).
Yang, H., Li, S.X., Liu, X.Y., 2013. Characteristics and resource prospects of tight oil and shale oil in Ordos basin. Acta Pet. Sin. 34, 1–11 (in Chinese with English abstract).
Yang, H., Zhang, W.Z., 2005. Leading effect of the seventh member high-quality source rock of Yanchang Formation in Ordos Basin during the enrichment of low-penetrating oil-gas accumulation: geology and geochemistry. Geochimica 34, 147–154 (in Chinese with English abstract).
Yang, H., Zhang, W., Wu, K., Li, S., Peng, P.A., Qin, Y., 2010. Uranium enrichment in lacustrine oil source rocks of the Chang 7 member of the Yanchang Formation, Erdos Basin, China. J. Asian Earth Sci. 39, 285–293.
Yang, J.J., 2002. Tectonic Evolution and Oil-gas Reservoirs Distribution in Ordos Basin. Petroleum Industry Press, Beijing, pp. 36–37 (in Chinese).
Yuan, W., Liu, G.D., Luo, W.B., 2016a. Deposition rate of the seventh member of Yanchang Formation, Ordos Basin and its impact on organic matter abundance of hydrocarbon source rock (Natural Science Edition). J. Xi'an Shiyou Uni. 31, 20–26 (in Chinese with English abstract).
Yuan, W., Liu, G.D., Stebbins, A., Xu, L.M., Niu, X.B., Luo, W.B., Li, C.Z., 2016b. Reconstruction of redox conditions during deposition of organic-rich shales of the upper triassic Yangchang formation, Ordos basin, China. Palaeogeogr. Palaeoclimatol. Palaeoecol. http://dx.doi.org/10.1016/j.palaeo.2016.12.020.
Zaback, D.A., Pratt, L.M., Hayes, J.M., 1993. Transport and reduction of sulfate and immobilization of sulfide in marine black shales. Geology 21, 141–144.
Zeng, S., Wang, J., Fu, X., Chen, W., Feng, X., Wang, D., Song, C., Wang, Z., 2015. Geochemical characteristics, redox conditions, and organic matter accumulation of marine oil shale from the Changliang Mountain area, northern Tibet, China. Mar. Petroleum Geol. 64, 203–221.
Zhang, W.Z., Yang, H., Peng, P.A., Yang, Y.H., Zhang, H., Shi, X.H., 2009. The influence of Late Triassic volcanism on the development of Chang7 high grade hydrocarbon source rock in Ordos Basin. Geochimica 38, 573–582 (in Chinese with English abstract).
Zhang, W.Z., Yang, H., Xie, L.Q., Yang, Y.H., 2010. Lake-bottom hydrothermal activities and their influences on the high-quality source rock development: a case from Chang 7 source rocks in Ordos Basin. Petroleum Explor. Dev. 424–429 (in Chinese with English abstract).
Zhang, W.Z., Yang, H., Yang, Y.H., Kong, Q.F., Wu, K., 2008. Petrology and element geochemistry and development environment of Yanchang Formation Chang 7 high quality source rocks in Ordos basin. Geochimica 37, 59–64 (in Chinese with English abstract).